Can a Musculoskeletal Model Adapted to Knee Implant Geometry Improve Prediction of 3D Contact Forces and Moments?

Sacha Guitteny, Rachid Aissaoui, Raphaël Dumas

Can a musculoskeletal model adapted to knee implant geometry improve prediction of 3D contact forces and moments?

Sacha Guitteny[a], Rachid Aissaoui[b], Raphael Dumas[a]

[a]Univ Lyon, Univ Claude Bernard Lyon 1, Univ Gustave Eiffel, LBMC UMR_T 9406, F-69622 Lyon, France

[b]Laboratoire de recherche en imagerie et orthopédie (LIO), Département Génie des systèmes, Ecole de technologie supérieure, Montréal, Canada

Abbreviated title: **Knee implant-adapted model for contact load predictions**

Correspondence:

Raphaël DUMAS

Telephone number: +33 4 72 14 23 56

Fax : +33 4 72 37 68 37

Email: raphael.dumas@univ-eiffel.fr

Abstract

Tibiofemoral contact loads are crucial parameters in the onset and progression of osteoarthrosis. While contact loads are frequently estimated from musculoskeletal models, their customization is often limited to scaling musculoskeletal geometry or adapting muscle lines. Moreover, studies have usually focused on superior-inferior contact force without investigating three-dimensional contact loads.

Using experimental data from six patients with instrumented total knee arthroplasty (TKA), this study customized a lower limb musculoskeletal model to consider the positioning and the geometry of the implant at knee level. Static optimization was performed to estimate tibiofemoral contact forces and contact moments as well as musculotendinous forces. Predictions from both a generic and a customized model were compared to the instrumented implant measurements.

Both models accurately predict superior-inferior (SI) force and abduction-adduction (AA) moment. Notably, the customization improves prediction of medial-lateral (ML) force and flexion-extension (FE) moments. However, there is subject-dependent variability in the prediction of anterior-posterior (AP) force.

The customized models presented here predict loads on all joint axes and in most cases improve prediction. Unexpectedly, this improvement was more limited for patients with more rotated implants, suggesting a need for further model adaptations such as muscle wrapping or redefinition of hip and ankle joint centers and axes.

Keywords

Osteoarthritis; musculoskeletal modeling; tibiofemoral contact loads; contact point location

Introduction

The distribution, intensity, and location of tibio-femoral (TF) contact forces are vital to the follow-up of osteoarthritis (OA) patients. Knee OA is a chronic disease characterized by joint cartilage damage affecting some 25% of people over 65 years old. Certain systemic factors have been identified, such as overweight, history of trauma, joint instability or muscular weakness leading to altered knee loads[42]. In vivo measurement of these TF contact forces is difficult, with instrumented total knee arthroplasty (TKA) remaining the sole method used. While this process yields data for comparison with reference data, the experimental protocols are extremely complex and invasive; it is really only feasible for a limited, older population with severe osteoarthritis.

This has led to the increasing use of non-invasive musculoskeletal modeling approaches[19]. Musculoskeletal models are based on the physiological representation of muscles and joints and on equations of motion. The models use inverse kinematics based only on the skeletal model to estimate joint kinematics, which can then be used to predict musculo-tendon and contact forces through inverse dynamic and static optimization. The literature has so far focused on gait analysis to compare experimental measurement from instrumented TKA and contact force estimation from musculoskeletal models, particularly addressing the superior-inferior direction. During gait, the root mean square errors (RMSE) ranged between 8.2%BW and 140%BW[41]. A few studies have analyzed the squat movement: Nejad et al. (2020)[25] finds an RMSE of 105.7%BW while Dumas and Moissenet (2020)[15] report an RMSE below 72%BW for the prediction of TF contact forces. Given the greater amplitude of knee flexion during the squat movement than during gait, the modeling of the knee joint would appear key to improving multibody optimization and joint kinematics estimation[8].

Different approaches have been suggested to model the knee joint. Ranging from simple to more complex, kinematic models represent the knee joint as a fixed or moving hinge[18,36], or define parallel mechanisms that take into account the mechanical behavior of simplified articular surfaces and ligaments[2,5,37,40]. An alternative method prescribes femoral and tibial medial and lateral trajectories of the contact points to describe knee joint kinematics[51]. Knee models with deformable parts (ligaments and cartilage) have also been proposed[9,23,27,30,36], considering the detailed articular surfaces and ligament as elastic; but these involve greater complexity of set-up, with numerous parameters to define and higher computational costs. Furthermore, subject-specific customization of the models is often limited to scaling the musculoskeletal geometry and adapting some muscle lines of action[7]. To the authors' knowledge, few musculoskeletal models have customized the kinematic model of the knee joint[15,21,53]. The impact of knee-joint customization on knee contact force prediction has not clearly been established: while it was reported to improve predictions in Gerus et al. (2013)[21], it did not show much effect in Dumas et al. (2020)[15]. The reason may be that previous studies assessed errors mainly regarding the superior-inferior component of TF contact force, whereas knee-joint customization may also impact prediction in other directions. Regardless of whether customized or generic models are used, errors on the other components of TF contact force are rarely studied[3,12,23,25,27]. The literature has focused on errors on medial and lateral superior-inferior contact forces, while errors on contact moments (including the other components of the forces as well as the 3D locations of contact points) have only been addressed in one study[27].

Yet, accurate knowledge of knee contact loads could improve analysis of factors involved in the longevity of TKA components, such as implant loosening and wear[1,33,48]. Polyethylene wear appears to depend on implant geometry and knee kinematics[4,38]. Moreover,

correlations between joint loads - including not only compressive forces but also flexion-extension and varus-valgus torque - and micromotions were documented in Fitzpatrick et al. (2014)[20]. A probabilistic model developed by Laz et al. (2006)[29] showed the effect of loading variability in anterior-posterior force and internal-external moments on implant performances.

The objective of this study is to evaluate subject-specific knee-joint models based on TKA kinematics and geometry in terms of TF contact forces and moments during both gait and squat movements. Implanting the TKA involves several modifications to TF and patellofemoral (PF) joints as well as some muscle lines of action. Contact point trajectories, PF hinge and tendon length, and wrapping cylinders are therefore customized. The predicted TF contact forces and moments are compared to the instrumented TKA measurements.

Materials and Methods

Dataset and processing

This study used the experimental data reported by Taylor et al. (2017)[44] (https://cams-knee.orthoload.com/). This dataset, called *CAMS-Knee*, provides kinematics and kinetics measurements of the lower limb musculoskeletal system during gait and squat for 6 subjects (5 males and 1 female, 68 ± 5years, 88 ± 12kg, 1.73 ± 0.04m) with instrumented TKA. The instrumented implant used was based on the INNEX knee (Zimmer GmbH, Winterthur, Switzerland), which features an ultra-congruent tibial insert and necessitates the removal of the cruciate ligaments. Measurements from one gait cycle were available for two of the six subjects, from two gait cycles for two other subjects, and from three gait cycles for the remaining subject included here. The gait data recorded for patient *K2R* were excluded

because the movement of the skin markers relative to their underlying bones appeared to be inconsistent. The six subjects were also measured during one squat cycle. The characteristics of the six CAMS-Knee subjects studied here are provided in Table 1.

Fluoroscopy-based implant position was recorded at 25Hz, skin marker motion was captured at 100Hz, and ground reaction forces were measured using force platforms at 2000Hz. All data were resampled to 100Hz; the fluoroscopic data were up-sampled using quaternion (*slerp*) interpolation. The raw data on skin marker position were gap-filled using QTM (Qualisys Track Manager) software; polynomial interpolations were used when the gap was less than 0.1s (10 frames), and the "relational/rigid body" method otherwise. The anatomical landmark positions of the shank and thigh segments and the skin markers on the foot and the pelvis were used to define the anatomical coordinate systems (CS) according to International Society of Biomechanics (ISB) recommendations[49]. All transformation matrices between the different CS, as well as CT-Scan anatomical landmarks, were provided by the authors.

Musculoskeletal modeling

A five-segment model (foot, tibia, patella, femur and pelvis), based on Delp et al. (1990)[10], with four joints, six joint degrees of freedom (DoF), and 43 muscle lines of action was developed for this study. All segments were positioned such that anatomical landmarks, joints, and muscle geometry were scaled to the subject anthropometry using the segment lengths. The model considered a spherical joint for the hip and a universal joint for the ankle. Two knee models were designed for purposes of comparison: a generic model and a customized one. Customization was directed at the knee, with the aim of assessing modification due to the positioning and geometry of the implant. The kinematic constraints of the TF joint were described with contact point trajectories[15,51] – either generic contact points derived from

kinematics described by Delp et al (1990)[10] or subject-specific contact points computed from fluoroscopy measurements during the squat movement[46]. The customized contact point trajectories in the transversal plane were obtained based on the study of Trepczynski et al. (2019)[46], which reported the anterior-posterior position of the lowest points of the femoral implant depending on the knee flexion-extension angle. The customized mediolateral position was defined such that it remained constant over the activity. These points were then projected onto the surface of the tibial implant to determine their superior-inferior position. Finally, contact points were defined in both femur and tibia bone segment coordinates systems and interpolated to the flexion range of each patient's gait cycle through fluoroscopic data. Contact point trajectories are illustrated in Figure 1. The patella-femoral (PF) joint was defined via either a generic [10] or a customized hinge joint. Location of the center and direction of the customized PF hinge joint were computed from the closest least square cylinder to the implant's trochlear part. When the customized model was used, the medio-lateral location of the patellar tendon insertion was shifted according to the tibial tuberosity landmark position. Patellar tendon length was set as the distance between tibial insertion and patella apex in a virtual standing posture with all CS segments aligned. The patellar tendon was assumed to be isometric. Finally, generic via points[10] were replaced by cylinders adjusted on the implant trochlear and condylar parts to wrap hamstring, quadriceps, and gastrocnemius muscle lines at knee level for the customized model. The knee model is depicted in Figure 2.

The position and orientation of the segments were estimated using a multibody kinematics optimization (MKO) approach that minimizes the sum of the squared distances between measured marker positions and those estimated by the model. The knee contact forces in both medial and lateral TF compartments and the musculo-tendon forces were calculated via one-step static optimization minimizing all the forces simultaneously[40]. The forces and moments

(i.e. forces multiplied by contact-level arms) predicted by the generic and customized models were compared to the instrumented TKA measurements in terms of coefficient of determination (R2), root mean square error (RMSE), and peak error. Predicted muscle forces were compared to the literature values obtained using static optimization and summarized in Trinler et al. (2018)[47].

Results

The customized model based on contact trajectories measured during squat and interpolated with flexion-extension angle predicted TF kinematics during gait that were close to the actual kinematics computed via fluoroscopic measurements. Figure 3 shows an example for subject K8L. Importantly, the generic model only provided the 3D kinematics of the joint in the sagittal plane.

The TF joint contact loads evaluated by both generic and customized models were compared to the forces and moments measured by the instrumented TKA. All force and moment measurements and predictions are shown for each patient during gait (Figure 4a and Figure 4b) and during a squat movement (Figure 6and Figure 6b). Table 2 and Table 3 (gait and squat, respectively) provide overviews of the results (R2, RMSE, and peak error) for each DoF averaged over the subjects. The prediction of superior-inferior (SI) forces during the squat movement was enhanced by customization, RMSE from 52%BW to 37%BW. For both generic and customized models as well as for both activities, R2 related to SI forces and abduction-adduction (AA) moments were high (R2 = 0.91 and 0.74 on average for the force predictions during gait and squat, respectively and R2=0.76 and 0.68 for the moment predictions). R2 related to anterior-posterior (AP) and medio-lateral (ML) forces and to flexion-extension (FE)

moments predicted by the customized model during gait were on average 0.11, 0.17, and 0.33, respectively, higher than from the generic model. However, the pattern of the ML force predictions remained inaccurate (R2 = 0.22 and R2 = 0.42 on average during gait and squat, respectively). The customized model delivered lower RMSE for AP forces and FE moments during gait (8%BW and 0.37%BW*Height on average). During squat, both models provided good prediction of AP forces (R2=0.77 and 0.73, RMSE= 15%BW and 14%BW for generic and customized model, respectively). Customized models appeared to better estimate peak knee loads in most of the degrees of freedom, especially for squat movement (data in Supplementary materials). The accuracy of AA moment prediction varied greatly according to subject; although both generic and customized models predicted moment values close to the implant measurements, the generic model provided better prediction for some subjects.

Figure 5 and Figure 8 show the average values for musculo-tendon forces computed with both models during gait and squat, respectively and for muscles surrounding the knee joint. During gait, hamstring and gastrocnemius forces were consistent with the values reported in the literature[47]. During squat movements, both generic and customized musculoskeletal models provided muscle force values for rectus femoris and hamstrings that differed from the literature[24]. Estimated vastii and rectus femoris forces showed the same pattern as that computed by previous authors; however, the force values found here were lower for both squat and gait movements. Forces computed for other muscles in the model are plotted and compared to data from Trinler et al. (2013)[47] and Nasab et al. (2022)[24] in Supplementary materials (Figure S3 and Figure S4).

Discussion

This study developed a musculoskeletal model featuring knee-joint customization based on implant kinematics and geometry. While other studies[21,53] adapted the kinematic constraints in the sagittal plane alone, the model developed here replicates the tibiofemoral kinematics in three dimensions by defining the contact point trajectories in space, as proposed by Zeighami et al. (2018)[51]. This allows the contact lever arms to be obtained directly, and the contact moments can be computed and compared to implant measurements.

This work assessed the ability of customized and generic models to evaluate knee contact loads during gait and squat movements by comparing them to instrumented TKA measurements. In addition to the SI force usually reported in the literature, 3D contact forces and moments were considered. The average RMSE of superior-inferior (SI) forces predicted with the generic model (RMSE = 44%BW on average) was comparable with that reported in Moissenet et al. (2017)[41] during gait. Although the customized model led to a slight increase in prediction errors on SI forces during gait (RMSE = 52%BW on average), the differences from measurement values remain within the range reported in the literature on knee-joint customization[15]. Prediction of SI forces during squat was improved using the customized model: SI forces appeared to be significantly less over-estimated than in previous studies[7,25] at deep knee flexion angles. During gait, peak SI force distribution between medial and lateral compartments was found similar to literature values obtained using instrumented implants (data in Supplementary materials). Moreover, total SI force magnitude was similar for gait and lower for squat relative to values reported by studies working with the CAMSknee dataset[24,25,43]. Finally, during squat movements, lateral peak SI forces were higher than medial peak SI forces, as reported by Bedo et al. (2020). Although AA moment prediction accuracy was subject-dependent, the RMSE was below the 1.5%BW*Height previously reported by Kia

et al. (2014)[27]. The coefficient of determination (R2) related to SI forces and abduction-adduction (AA) moments was similar to literature values during gait[25].

Looking at other DoFs, RMSE on AP and ML forces fell within the low error range reported in the literature during gait [3,23,27]and FE moment predictions were similar to the estimations of Kia et al. (2014)[27]. The improvement in FE moment prediction is likely due to enhanced tracking of the AP translation and IER, with notable differences between the two models shown in Figure 3 and Figure 6. These changes should modify the AP moment arm during knee flexion. The predictions yielded by this customized musculoskeletal model therefore appear both to fall within the range of values reported in the literature for the commonly assessed SI direction and to be consistent with the few reported assessments for most of the other directions. This indicates that the method delivers results comparable to implant load measurements.

Unexpectedly, the improvement from customization was more limited for some subjects, with a reduction in prediction accuracy on ML forces and AA moments in specific cases, like subjects K3R and K5R during squat. This effect could be due to the implant being more rotated than the anatomical CS.

The computed knee muscle forces were similar to or in the low range of literature values[47]. The approaches reviewed in Trinler et al. (2013)[47] generally minimized activation alone. The low muscle force values observed here therefore appear consistent with the simultaneous minimization of TF contact forces in one-step static optimization. Minimizing musculo-tendon forces or muscle activations simultaneously with contact forces appears to be a widely adopted approach[11,15,34,35,40,50].

The musculoskeletal modeling presented here involves some limitations. Although the model's aim was to customize the patellofemoral joint, the position of the patella segments

remains inaccurate. Using CT images the patella landmark digitization could be improved since fluoroscopic images are not currently available. The PF joint has been shown to play a major role in knee loading, particularly at deep flexion angles[26,45]. This makes patella position important, as it governs the patellar tendon and quadriceps orientations. Furthermore, the tibiofemoral contact position was customized to enable prediction of the actual tibiofemoral kinematics. The contact points were determined based on contact trajectories obtained from squat movements and were also used to analyze tibiofemoral joint behavior during gait. It is worth noting that these contact points can vary depending on the type of activity. However, previous studies by Varadarajan et al. (2008)[48], Kour et al., (2022)[28], and Byrapogu et al., (2023)[6] did not find major differences in contact locations between various daily activities (such as lunging, level walking, downhill walking, stair descent and ascent) for TKA subjects. Moreover, subjects had very similar trajectories, due to having the same implant geometry, as reported by Dumas et Moissenet (2020)[15] while using another TKA design. However, subjects' tibiofemoral loads differed and this suggests that knee-level customization alone (including wrapping cylinders only for some muscles surrounding the knee) may not be sufficient to account for subject variability. Indeed, the investigation by Hosseini Nasab et al. (2022)[24] demonstrated significant modifications of tibiofemoral loads based on musculo-tendon geometry (muscle pathways) and parameters (maximum isometric force), while Nejad et al. (2020)[25] found that adjusting muscle wrapping around the hip helps to reduce predicted muscle forces during deep flexion. In addition, this study did not model the collateral ligaments, which could limit the accuracy of prediction of TF loads, especially for AA moments. Finally, there were some discrepancies in the model's predictions. Customized models appeared to worsen predictions of TF load in some DoFs for subject K1L, while they improved predictions for the other subjects. For this particular subject's contact locations, the

trajectories were similar using both generic and customized models, which may explain the lack of improvement in TF load prediction. Note also that subject K1L had the weakest posterior tibial slope (5° as opposed to 7° to 11° for the other subjects).

Further adaptations might enhance the performance of such customized models. More detailed customization of the patellofemoral joint could improve prediction of joint loading during movements with deeper knee flexion. Improving ankle- and hip-joint modeling with subject-specific customization would also certainly be beneficial[39]. In contrast, a simplified tibiofemoral contact model could feasibly provide knee-joint customization for TKA patients. This model would be based solely on implant curvatures, the only difference between subjects being the posterior slope and axial rotation of the implant resulting from the surgery. This approach could avoid the need for dynamic fluoroscopy trials. Finally, prediction accuracy might be improved by adding via points to enhance the wrapping of the muscle action lines, or modifying the coordinates of their insertions and origins, or looking at the geometry of other strong muscles like the gluteus maximus.

This study suggests that knee-joint model customization based on implant kinematics and geometry could improve predictions of tibiofemoral loads. This holds promise for OA or obese populations, in which a shift in medial direction for medial and lateral contact points has been noted[32,52]. Moreover, after TKA, contact point locations appear to be lateralized again[32] and TKA design may impact the contact point trajectories[22]. Previous studies have shown that altering the location of contact points in the medial and lateral compartments of the tibiofemoral joint affects the distribution of contact force[16,31].

An improved understanding of 3D loads can enhance the design and development of implants by providing an accurate picture of in vivo loading mechanisms, which might prevent implant failures such as aseptic loosening or component wear[1,33]. In addition to improvements in TKA

design and assessment, insights into the onset and progression of OA could be gained by observing 3D tibiofemoral loads. Such knowledge would be useful in a clinical setting for OA prevention.

Acknowledgment

This study was partially financed by Région Auvergne Rhône Alpes (PAI 2021).

We thank Marjorie Sweetko for English language editing.

Conflict of Interest statement

The authors do not have any financial or personal relationships with other people or organizations that have inappropriately influenced this study.

References

1. Au, A. G., V. James Raso, A. B. Liggins, and A. Amirfazli. Contribution of loading conditions and material properties to stress shielding near the tibial component of total knee replacements. *J. Biomech.* 40:1410–1416, 2007.
2. Barzan, M., L. Modenese, C. P. Carty, S. Maine, C. A. Stockton, N. Sancisi, A. Lewis, J. Grant, D. G. Lloyd, and S. Brito da Luz. Development and validation of subject-specific pediatric multibody knee kinematic models with ligamentous constraints. *J. Biomech.* 93:194–203, 2019.
3. Bennett, K. J., C. Pizzolato, S. Martelli, J. S. Bahl, A. Sivakumar, G. J. Atkins, L. Bogdan Solomon, and D. Thewlis. EMG-Informed Neuromusculoskeletal Models Accurately Predict Knee Loading Measured Using Instrumented Implants. *IEEE Trans. Biomed. Eng.* 69:2268–2275, 2022.
4. Blunn, G. W., A. B. Joshi, R. J. Minns, L. Lidgren, P. Lilley, L. Ryd, E. Engelbrecht, and P. S. Walker. Wear in retrieved condylar knee arthroplasties. *J. Arthroplasty* 12:281–290, 1997.
5. Brito da Luz, S., L. Modenese, N. Sancisi, P. M. Mills, B. Kennedy, B. R. Beck, and D. G. Lloyd. Feasibility of using MRIs to create subject-specific parallel-mechanism joint models. *J. Biomech.* 53:45–55, 2017.
6. Byrapogu, V., T. Gale, L. Dukens, B. Hamlin, K. L. Urish, and W. Anderst. How well does intra-operative contact path predict post-operative contact path during activities of daily living. *Med. Eng. Phys.* 111:103948, 2023.
7. Catelli, D. S., M. Wesseling, I. Jonkers, and M. Lamontagne. A musculoskeletal model customized for squatting task. *Comput. Methods Biomech. Biomed. Engin.* 22:21–24, 2019.
8. Clément, J., R. Dumas, N. Hagemeister, and J. A. de Guise. Soft tissue artifact compensation in knee kinematics by multi-body optimization: Performance of subject-specific knee joint models. *J. Biomech.* 48:3796–3802, 2015.
9. Dejtiar, D. L., C. M. Dzialo, P. H. Pedersen, K. K. Jensen, M. K. Fleron, and M. S. Andersen. Development and Evaluation of a Subject-Specific Lower Limb Model With an Eleven-Degrees-of-Freedom Natural Knee Model Using Magnetic Resonance and Biplanar X-Ray Imaging During a Quasi-Static Lunge. *J. Biomech. Eng.* 142:061001, 2020.
10. Delp, S. L., J. P. Loan, M. G. Hoy, F. E. Zajac, E. L. Topp, and J. M. Rosen. An interactive graphics-based model of the lower extremity to study orthopaedic surgical procedures. *IEEE Trans. Biomed. Eng.* 37:757–767, 1990.
11. DeMers, M. S., S. Pal, and S. L. Delp. Changes in tibiofemoral forces due to variations in muscle activity during walking: Tibiofemoral forces and muscle activity. *J. Orthop. Res.* 32:769–776, 2014.
12. Dumas, R., A. Barré, F. Moissenet, and R. Aissaoui. Can a reduction approach predict reliable joint contact and musculo-tendon forces? *J. Biomech.* 95:109329, 2019.
13. Dumas, R., and L. Chèze. 3D inverse dynamics in non-orthonormal segment coordinate system. *Med. Biol. Eng. Comput.* 45:315–322, 2007.
14. Dumas, R., L. Cheze, and F. Moissenet. Multibody Optimisations: From Kinematic Constraints to Knee Contact Forces and Ligament Forces. In: Biomechanics of Anthropomorphic Systems, edited by G. Venture, J.-P. Laumond, and B. Watier. Cham: Springer International Publishing, 2019, pp. 65–89.
15. Dumas, R., and F. Moissenet. Accuracy of the tibiofemoral contact forces estimated by a subject-specific musculoskeletal model with fluoroscopy-based contact point trajectories. *J. Biomech.* 113:110117, 2020.

16. Dumas, R., A. Zeighami, and R. Aissaoui. Knee Medial and Lateral Contact Forces Computed Along Subject-Specific Contact Point Trajectories of Healthy Volunteers and Osteoarthritic Patients. In: Computer Methods, Imaging and Visualization in Biomechanics and Biomedical Engineering, edited by G. A. Ateshian, K. M. Myers, and J. M. R. S. Tavares. Cham: Springer International Publishing, 2020, pp. 457–463.
17. Duprey, S., L. Cheze, and R. Dumas. Influence of joint constraints on lower limb kinematics estimation from skin markers using global optimization. *J. Biomech.* 43:2858–2862, 2010.
18. Dzialo, C. M., P. H. Pedersen, K. K. Jensen, M. de Zee, and M. S. Andersen. Evaluation of predicted patellofemoral joint kinematics with a moving-axis joint model. *Med. Eng. Phys.* 73:85–91, 2019.
19. Erdemir, A., S. McLean, W. Herzog, and A. J. van den Bogert. Model-based estimation of muscle forces exerted during movements. *Clin. Biomech.* 22:131–154, 2007.
20. Fitzpatrick, C. K., P. Hemelaar, and M. Taylor. Computationally efficient prediction of bone–implant interface micromotion of a cementless tibial tray during gait. *J. Biomech.* 47:1718–1726, 2014.
21. Gerus, P., M. Sartori, T. F. Besier, B. J. Fregly, S. L. Delp, S. A. Banks, M. G. Pandy, D. D. D'Lima, and D. G. Lloyd. Subject-specific knee joint geometry improves predictions of medial tibiofemoral contact forces. *J. Biomech.* 46:2778–2786, 2013.
22. Gray, H. A., S. Guan, T. Young, M. Dowsey, P. Choong, and M. Pandy. Comparison of posterior- stabilized cruciate- retaining and medial- stabilized. *J. Orthop. Res.* 38:1753–1768, 2020.
23. Hast, M. W., and S. J. Piazza. Dual-Joint Modeling for Estimation of Total Knee Replacement Contact Forces During Locomotion. *J. Biomech. Eng.* 135:021013, 2013.
24. Hosseini Nasab, S. H., C. R. Smith, A. Maas, A. Vollenweider, J. Dymke, P. Schütz, P. Damm, A. Trepczynski, and W. R. Taylor. Uncertainty in Muscle–Tendon Parameters can Greatly Influence the Accuracy of Knee Contact Force Estimates of Musculoskeletal Models. *Front. Bioeng. Biotechnol.* 10:808027, 2022.
25. Imani Nejad, Z., K. Khalili, S. H. Hosseini Nasab, P. Schütz, P. Damm, A. Trepczynski, W. R. Taylor, and C. R. Smith. The Capacity of Generic Musculoskeletal Simulations to Predict Knee Joint Loading Using the CAMS-Knee Datasets. *Ann. Biomed. Eng.* 48:1430–1440, 2020.
26. Kebbach, M., M. Darowski, S. Krueger, C. Schilling, T. M. Grupp, R. Bader, and A. Geier. Musculoskeletal Multibody Simulation Analysis on the Impact of Patellar Component Design and Positioning on Joint Dynamics after Unconstrained Total Knee Arthroplasty. *Materials* 13:2365, 2020.
27. Kia, M., A. P. Stylianou, and T. M. Guess. Evaluation of a musculoskeletal model with prosthetic knee through six experimental gait trials. *Med. Eng. Phys.* 36:335–344, 2014.
28. Kour, R. Y. N., S. Guan, M. M. Dowsey, P. F. Choong, and M. G. Pandy. Kinematic function of knee implant designs across a range of daily activities. *J. Orthop. Res.* jor.25476, 2022.
29. Laz, P. J., S. Pal, A. Fields, A. J. Petrella, and P. J. Rullkoetter. Effects of knee simulator loading and alignment variability on predicted implant mechanics: A probabilistic study. *J. Orthop. Res.* 24:2212–2221, 2006.
30. Lenhart, R. L., J. Kaiser, C. R. Smith, and D. G. Thelen. Prediction and Validation of Load-Dependent Behavior of the Tibiofemoral and Patellofemoral Joints During Movement. *Ann. Biomed. Eng.* 43:2675–2685, 2015.
31. Lerner, Z. F., M. S. DeMers, S. L. Delp, and R. C. Browning. How tibiofemoral alignment and contact locations affect predictions of medial and lateral tibiofemoral contact forces. *J. Biomech.* 48:644–650, 2015.

32. Li, J., T. Tsai, M. M. Clancy, C. L. Lewis, D. T. Felson, and G. Li. Cartilage contact characteristics of the knee during gait in individuals with obesity. *J. Orthop. Res.* 40:2480–2487, 2022.
33. Liau, J.-J., C.-K. Cheng, C.-H. Huang, and W.-H. Lo. The effect of malalignment on stresses in polyethylene component of total knee prostheses – a finite element analysis. *Clin. Biomech.* 17:140–146, 2002.
34. Lin, Y., J. Walter, S. Banks, M. Pandy, and B. J. Fregly. Simultaneously prediction of muscle and contact forces in the knee during gait. *J. Biomech.* 43:945–952, 2010.
35. Manal, K., and T. S. Buchanan. An Efficient One-Step Moment Balancing Algorithm for Computing Medial and Lateral Knee Compartment Contact Forces. *J. Biomech. Eng.* 144:034501, 2022.
36. Marra, M. A., V. Vanheule, R. Fluit, B. H. F. J. M. Koopman, J. Rasmussen, N. Verdonschot, and M. S. Andersen. A Subject-Specific Musculoskeletal Modeling Framework to Predict In Vivo Mechanics of Total Knee Arthroplasty. *J. Biomech. Eng.* 137:020904, 2015.
37. Martelli, S., N. Sancisi, M. Conconi, M. G. Pandy, M. E. Kersh, V. Parenti-Castelli, and K. J. Reynolds. The relationship between tibiofemoral geometry and musculoskeletal function during normal activity. *Gait Posture* 80:374–382, 2020.
38. McEwen, H. M. J., P. I. Barnett, C. J. Bell, R. Farrar, D. D. Auger, M. H. Stone, and J. Fisher. The influence of design, materials and kinematics on the in vitro wear of total knee replacements. *J. Biomech.* 38:357–365, 2005.
39. Modenese, L., M. Barzan, and C. P. Carty. Dependency of lower limb joint reaction forces on femoral version. *Gait Posture* 88:318–321, 2021.
40. Moissenet, F., L. Chèze, and R. Dumas. A 3D lower limb musculoskeletal model for simultaneous estimation of musculo-tendon, joint contact, ligament and bone forces during gait. *J. Biomech.* 47:50–58, 2014.
41. Moissenet, F., L. Modenese, and R. Dumas. Alterations of musculoskeletal models for a more accurate estimation of lower limb joint contact forces during normal gait: A systematic review. *J. Biomech.* 63:8–20, 2017.
42. Saxby, D. J., and D. G. Lloyd. Osteoarthritis year in review 2016: mechanics. *Osteoarthritis Cartilage* 25:190–198, 2017.
43. Schellenberg, F., W. R. Taylor, A. Trepczynski, R. List, I. Kutzner, P. Schütz, G. N. Duda, and S. Lorenzetti. Evaluation of the accuracy of musculoskeletal simulation during squats by means of instrumented knee prostheses. *Med. Eng. Phys.* 61:95–99, 2018.
44. Taylor, W. R., P. Schütz, G. Bergmann, R. List, B. Postolka, M. Hitz, J. Dymke, P. Damm, G. Duda, H. Gerber, V. Schwachmeyer, S. H. Hosseini Nasab, A. Trepczynski, and I. Kutzner. A comprehensive assessment of the musculoskeletal system: The CAMS-Knee data set. *J. Biomech.* 65:32–39, 2017.
45. Trepczynski, A., I. Kutzner, E. Kornaropoulos, W. R. Taylor, G. N. Duda, G. Bergmann, and M. O. Heller. Patellofemoral joint contact forces during activities with high knee flexion. *J. Orthop. Res.* 30:408–415, 2012.
46. Trepczynski, A., I. Kutzner, P. Schütz, J. Dymke, R. List, P. von Roth, P. Moewis, G. Bergmann, W. R. Taylor, and G. N. Duda. Tibio-Femoral Contact Force Distribution is Not the Only Factor Governing Pivot Location after Total Knee Arthroplasty. *Sci. Rep.* 9:182, 2019.
47. Trinler, U., K. Hollands, R. Jones, and R. Baker. A systematic review of approaches to modelling lower limb muscle forces during gait: Applicability to clinical gait analyses. *Gait Posture* 61:353–361, 2018.

48. Varadarajan, K. M., A. L. Moynihan, D. D'Lima, C. W. Colwell, and G. Li. In vivo contact kinematics and contact forces of the knee after total knee arthroplasty during dynamic weight-bearing activities. *J. Biomech.* 41:2159–2168, 2008.
49. Wu, G., S. Siegler, P. Allard, C. Kirtley, A. Leardini, D. Rosenbaum, M. Whittle, D. D. D'Lima, L. Cristofolini, H. Witte, O. Schmid, and I. Stokes. ISB recommendation on definitions of joint coordinate system of various joints for the reporting of human joint motion—part I: ankle, hip, and spine. *J. Biomech.* 35:543–548, 2002.
50. Zargham, A., M. Afschrift, J. De Schutter, I. Jonkers, and F. De Groote. Inverse dynamic estimates of muscles recruitment and joint contact forces are more realistic when minimizing muslce activity rather than metabolic energy or contact forces. *Gait Posture* 74:223–230, 2019.
51. Zeighami, A., R. Aissaoui, and R. Dumas. Knee medial and lateral contact forces in a musculoskeletal model with subject-specific contact point trajectories. *J. Biomech.* 69:138–145, 2018.
52. Zeighami, A., R. Dumas, M. Kanhonou, N. Hagemeister, F. Lavoie, J. A. de Guise, and R. Aissaoui. Tibio-femoral joint contact in healthy and osteoarthritic knees during quasi-static squat: A bi-planar X-ray analysis. *J. Biomech.* 53:178–184, 2017.
54. Zhang, L., G. Liu, Y. Yan, B. Han, H. Li, J. Ma, and X. Wang. A subject-specific musculoskeletal model to predict the tibiofemoral contact forces during daily living activities. *Comput. Methods Biomech. Biomed. Engin.* 1–14, 2022.

Table & figure captions:

Figure 1: Transversal and sagittal views of the tibia and femoral components, respectively, with contact point trajectories for each patient obtained during gait and squat using both generic (blue dots) and customized (red dots) models. TF anatomical axes relative to the implant are computed from CT scan landmarks given in the dataset. Figures for patients K1L, K7L, and K8L (with a left prosthesis) have been symmetrized.

Figure 2: TKA customized model with medial and lateral contact points (red dots), patella-femoral hinge axis position and direction (purple star and arrow), patellar tendon (pink) and muscle wrapping cylinders (orange and red).

Figure 3: Example of tibio-femoral kinematics in all six degrees of freedom during one gait cycle of one subject (K8L) - fluoroscopic measurement (black), generic model (blue), and customized model predictions (red)

Figure 4a: Tibio-femoral forces during gait cycles of each subject – instrumented TKA (black), generic model (blue), and customized model predictions (red). One standard deviation intervals were plotted when several gait cycles were available.

Figure 4b: Tibio-femoral moments during gait cycles of each subject - instrumented TKA (black), generic model (blue), and customized model predictions (red). One standard deviation intervals were plotted when several gait cycles were available.

Figure 5: Knee-crossing muscle forces on average for all subjects during one gait cycle – Trinler et al. (2018) (black), generic model (blue), and customized model predictions (red). One standard deviation intervals were plotted.

Figure 6: Example of tibio-femoral kinematics in all six degrees of freedom during one squat movement of one subject (K8L) - fluoroscopic measurement (black), generic model (blue), and customized model predictions (red).

Figure 7a: Tibio-femoral forces during squat movements of each subject – instrumented TKA (black), generic model (blue), and customized model predictions (red).

Figure 7b: Tibio-femoral moments during squat movements of each subject – instrumented TKA (black), generic model (blue), and customized model predictions (red).

Figure 8: Knee-crossing muscle forces for each subject during squat movements – Nasab et al. (2022) (black), generic model (blue), and customized model predictions (red).

Table 1: Anthropometrics of patients in the *CAMS-Knee* dataset

Table 2: Coefficients of determination (R2) and root mean square errors (RMSE) in all degrees of freedom, during gait cycle: instrumented TKA measurements compared with both generic and customized model prediction.

Table 3: Coefficients of determination (R2) and root mean square errors (RMSE) in all degrees of freedom, during squat movement: instrumented TKA measurements compared with both generic and customized model prediction.

Figure 1

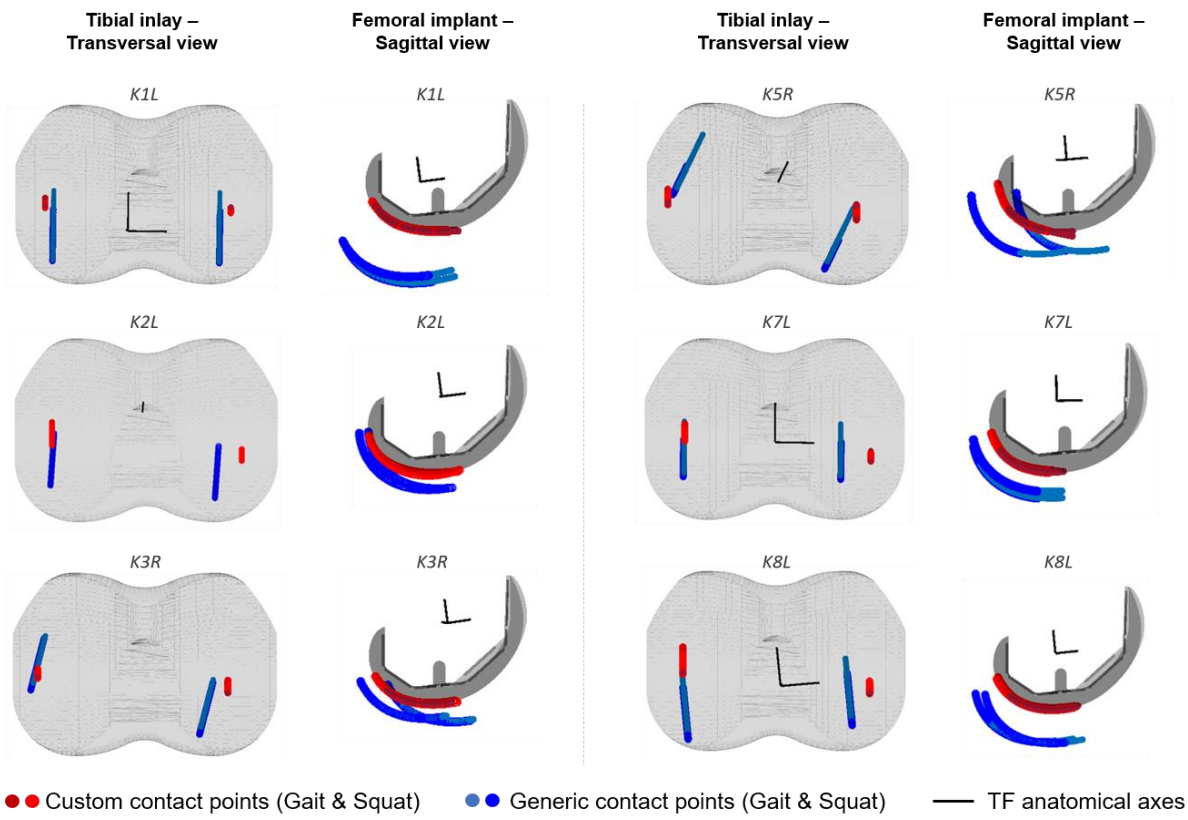

Figure 2

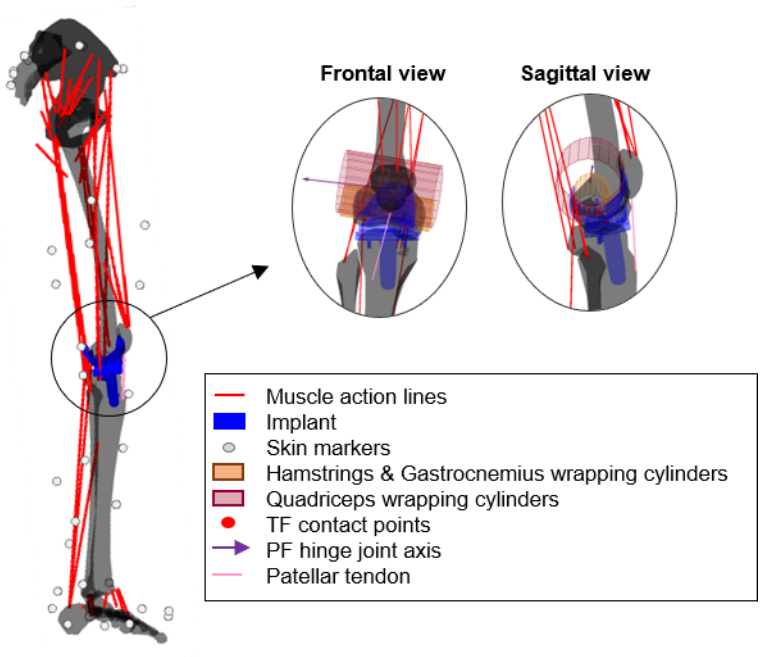

Figure 3

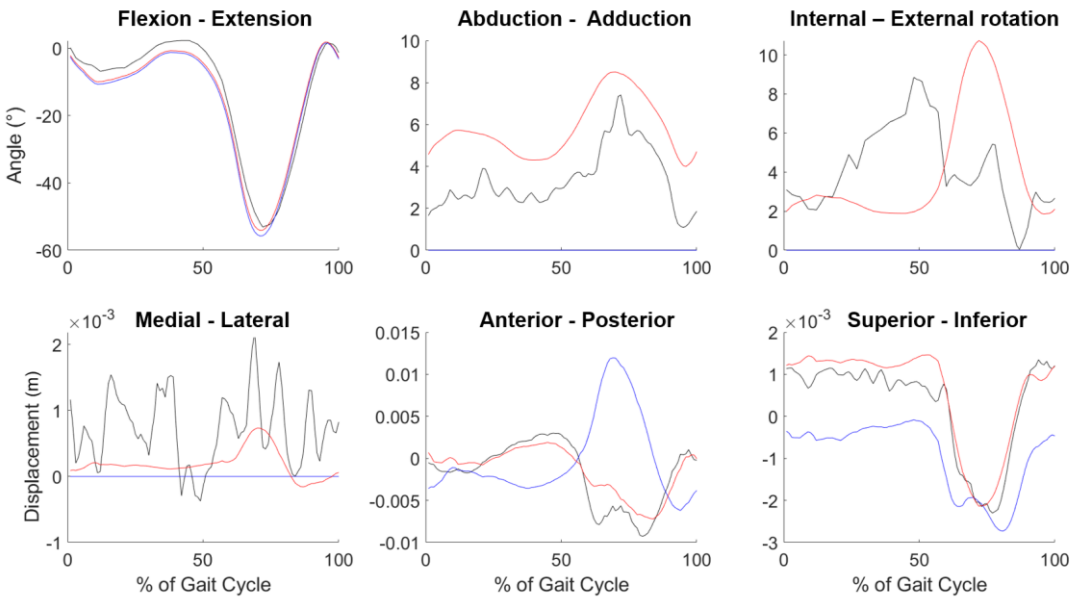

Figure 4a

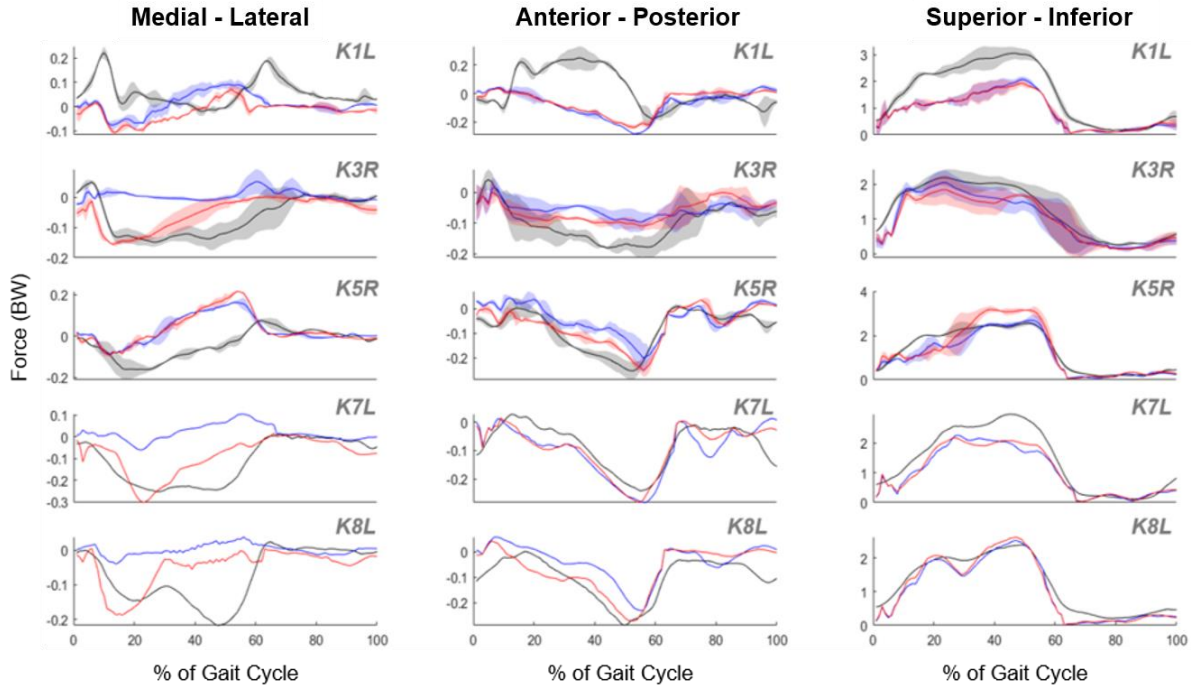

Figure 4b

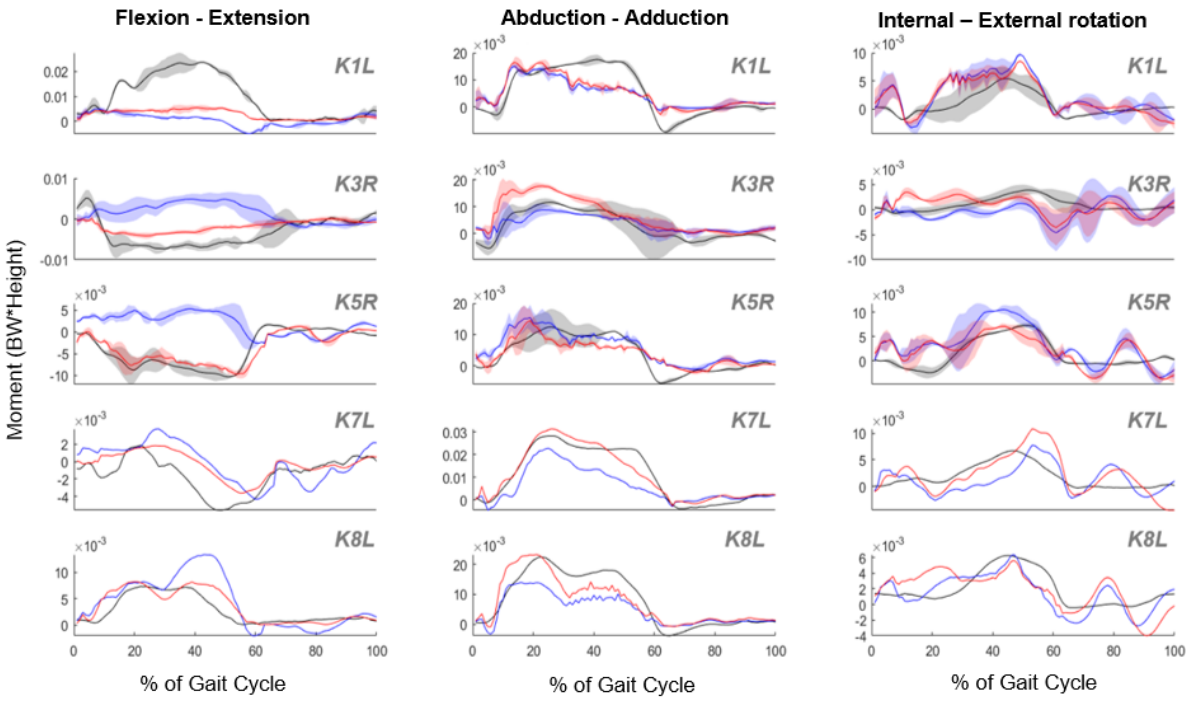

Figure 5

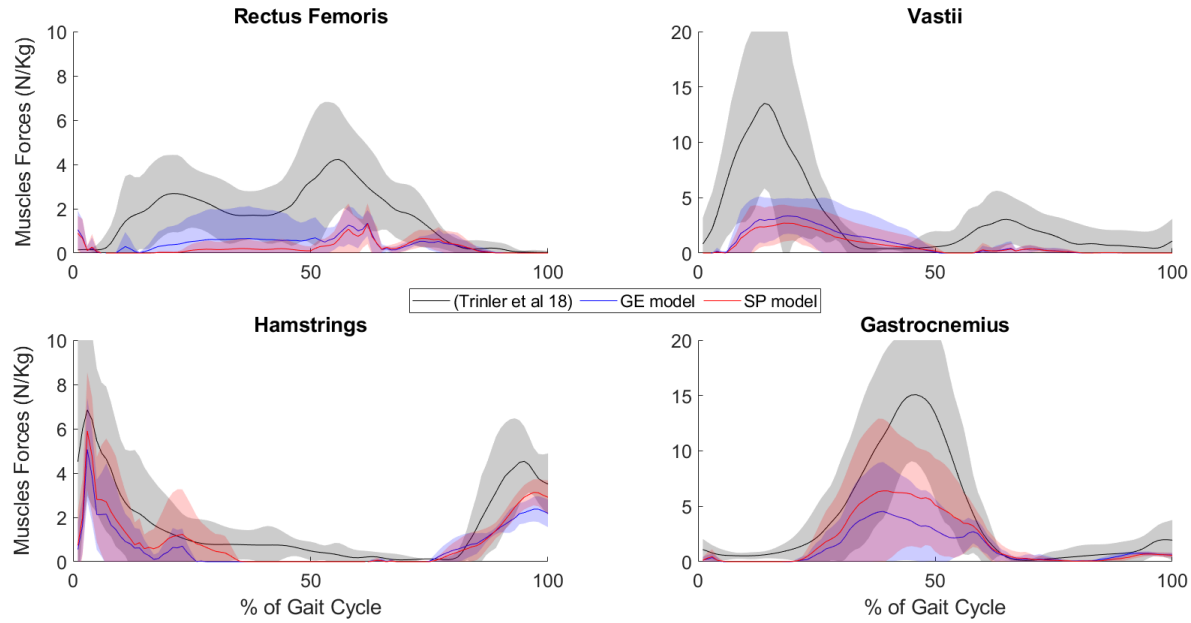

Figure 6 :

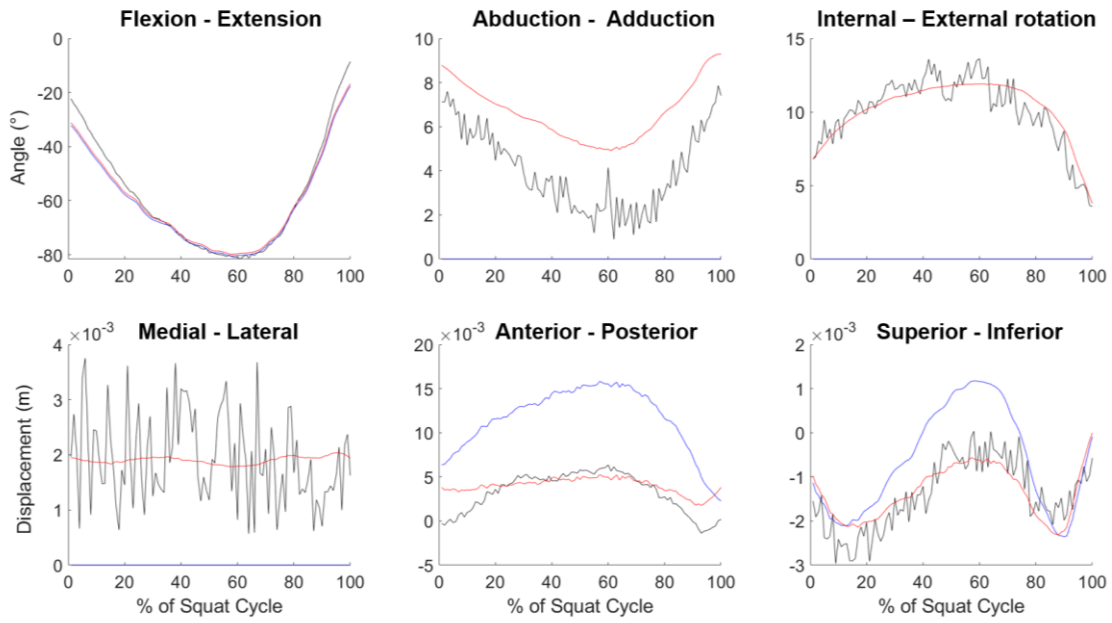

Figure 7a :

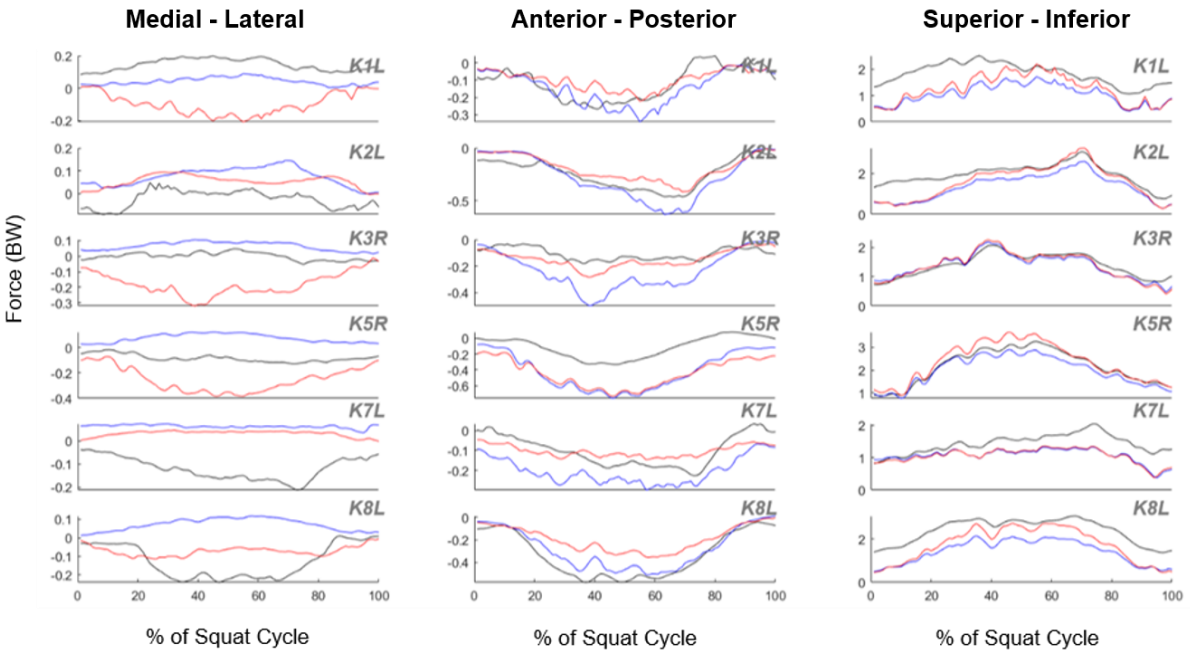

Figure 7b :

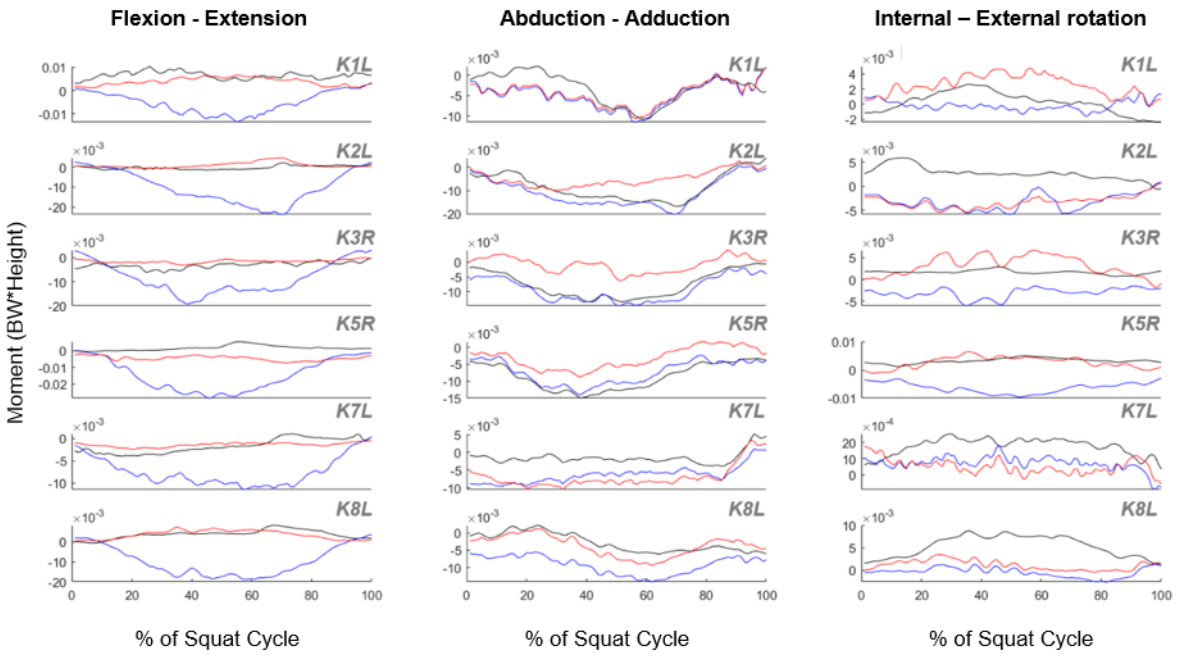

Figure 8 :

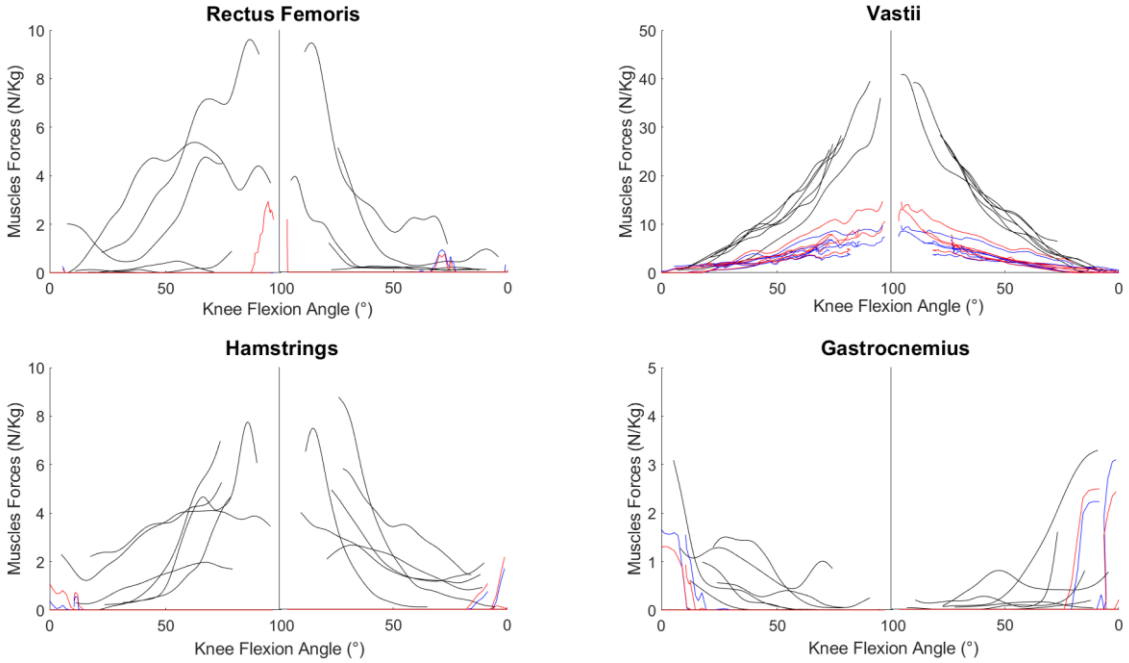

Table 1 :

	K1L	K2L	K3R	K5R	K7L	K8L
Gender	Male	Male	Male	Male	Female	Male
Prosthesis side	Left	Left	Right	Right	Left	Left
Age (years)	70	78	77	65	80	76
Mass (Kg)	101.5	90.8	100.3	95.6	66.5	78.8
Height (cm)	175	169	173	174	165	175

Table 2 :

R^2	AP	SI	ML	AA	IE	FE
Generic	0.48	0.94	0.05	0.77	0.36	0.38
Customized	0.59	0.92	0.22	0.75	0.32	0.71
RMSE (in BW and BW*Height)						
Generic	0.10	0.44	0.12	5.1e-3	2.7e-3	6.9e-3
Customized	0.08	0.52	0.09	4.2e-3	2.7e-3	3.7e-3

Table 3 :

R^2	AP	SI	ML	AA	IE	FE
Generic	0.77	0.75	0.46	0.69	0.35	0.20
Customized	0.73	0.73	0.42	0.67	0.24	0.24
RMSE (in BW and BW*Height)						
Generic	0.15	0.52	0.15	3.7e-3	4.9e-3	12.6e-3
Customized	0.14	0.37	0.18	4.7e-3	2.7e-3	3.0e-3

Supplementary materials

Figure S1: Peak forces and moments (described in Bergman et al. 2014) for all subjects during gait cycles – instrumented TKA measurements (black), generic model (blue), and customized model (red) predictions.

Figure S2: Peak forces and moments (described in Bergman et al. 2014) for all subjects during squat movements – instrumented TKA measurements (black), generic model (blue), and customized model (red) predictions.

Figure S3: Lower limb muscle forces on average for all subjects during one gait cycle – Trinler et al. (2018) (black), generic model (blue), and customized model predictions (red). One standard deviation intervals were plotted.

Figure S4: Lower limb muscle forces for each subject during squat movements – Nasab et al. (2022) (black), generic model (blue), and customized model predictions (red).

Table S1: Errors in mean peak forces and moments for all subjects during gait cycles for both generic and customized models.

Table S2: Errors in mean peak forces and moments for all subjects during squat movements for both generic and customized models.

Table S3: Medial and Lateral knee peak load distribution during gait cycles for each subject. Comparison with literature reports.

Table S4: Medial and Lateral knee peak load distribution during squat movements for each subject. Comparison with literature reports.

Appendix A – Computational framework adapted from [14,40,51]

Figure S1:

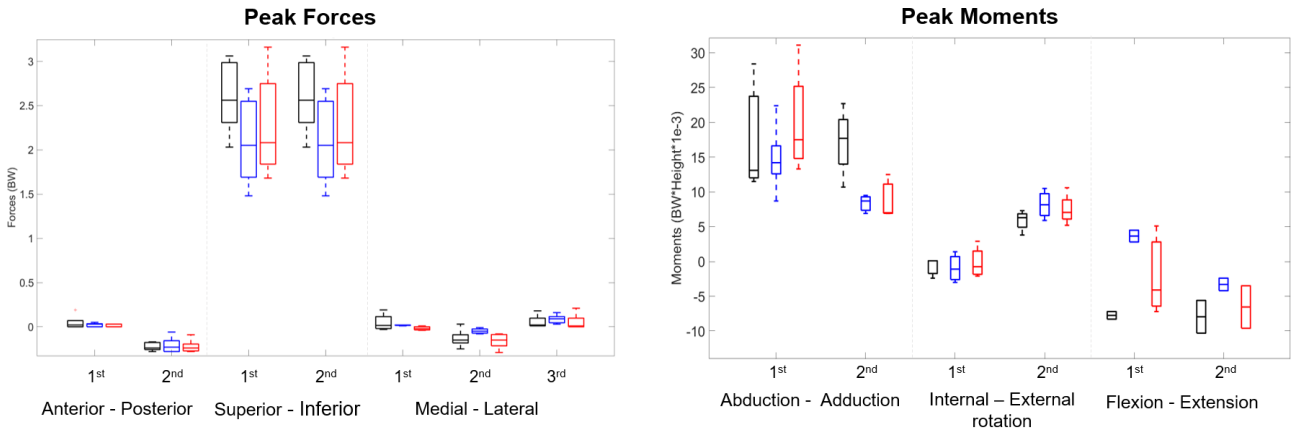

Figure S2:

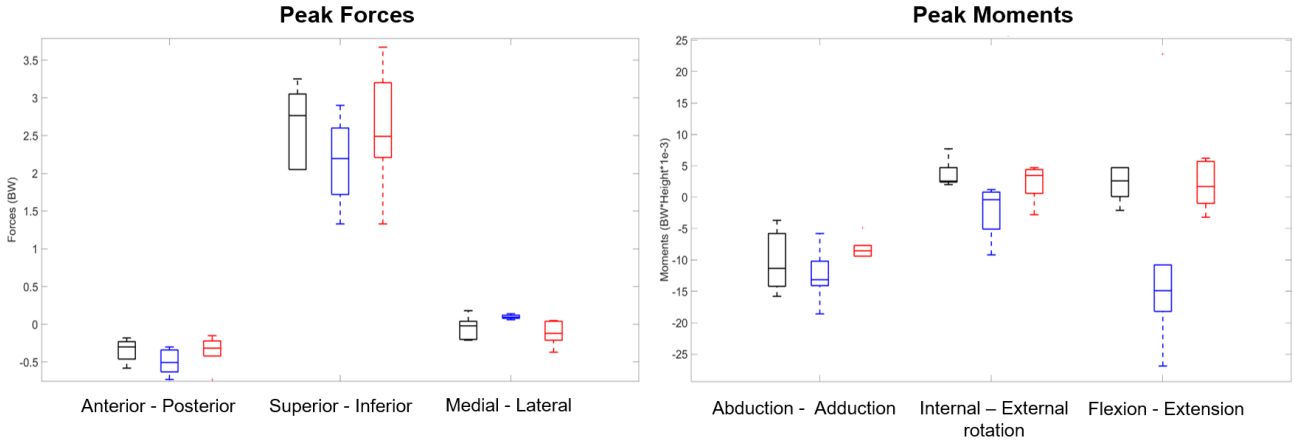

Figure S3:

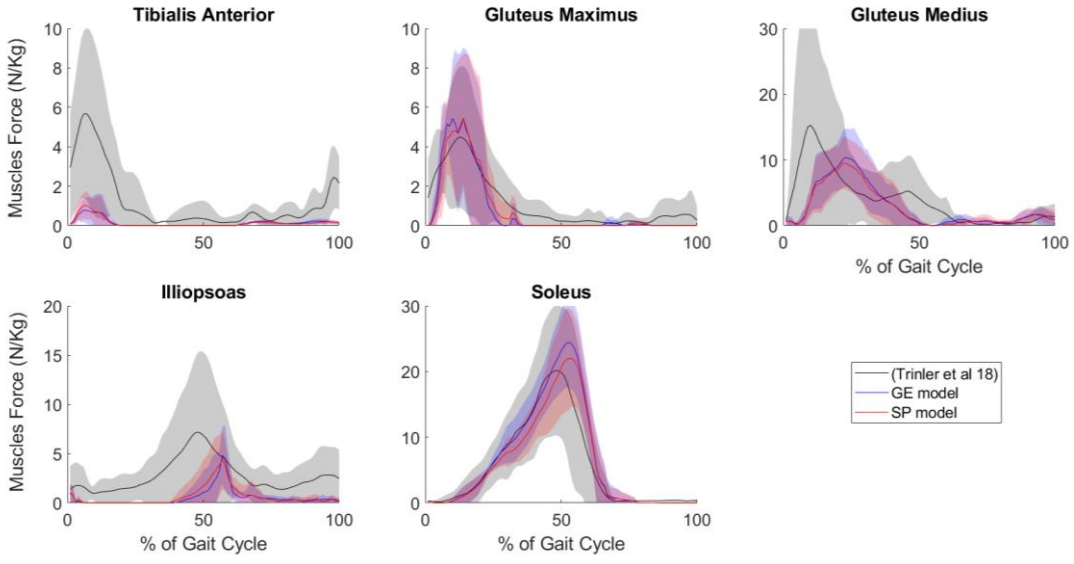

Figure S4:

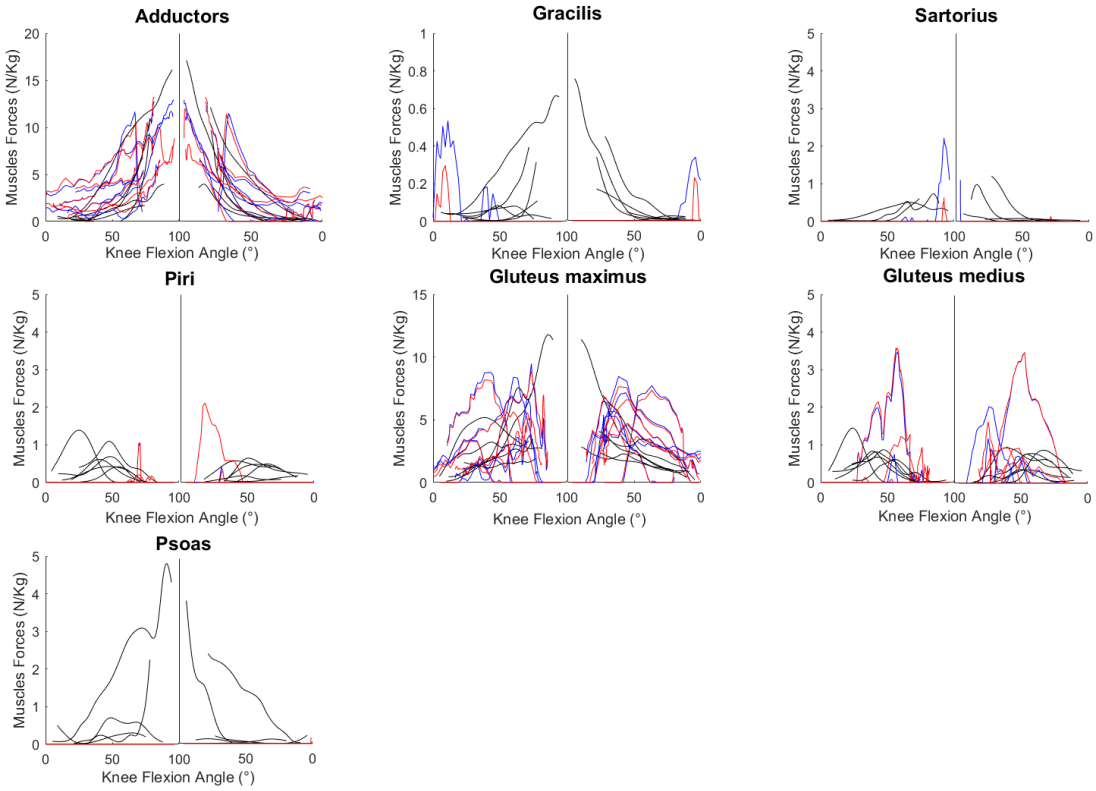

Table S1:

Mean peak errors (BW and BW*Height)							
	AP		**SI**		**ML**		
	1st	**2nd**	**1st**	**2nd**	**1st**	**2nd**	**3rd**
Generic	0.08	0.08	0.23	0.75	0.09	0.13	0.07
Customized	0.07	0.05	0.32	0.73	0.09	0.07	0.08
	AA		**IER**		**FE**		
	1st	**2nd**	**1st**	**2nd**	**1st**	**2nd**	
Generic	4.9e-3	8.1e-3	2.1e-3	2.8e-3	9.4e-3	5.1e-3	
Customized	3.2e-3	7.1e-3	1.9e-3	2.6e-3	2.1e-3	0.6e-3	

Table S2:

Mean peak errors (BW and BW*Height)						
	AP	SI	**ML**	AA	**IER**	FE
Generic	0.55	1.52	0.48	8.8e-3	17.9e-3	50.9e-3
Customized	0.48	0.98	0.6	13.3e-3	7.6e-3	8.9e-3

Table S3:

		Medial		Lateral		Total	
		1st	2nd	1st	2nd	1st	2nd
K1L	*Generic*	1.11	1.36	0.28	0.66	n/a	2.05
	Customized	1.17	1.27	0.28	0.62	n/a	1.89
K3R	*Generic*	1.33	n/a	0.72	n/a	2.02	1.48
	Customized	1.53	n/a	0.27	0.52	1.82	1.68
K5R	*Generic*	1.31	1.81	0.22	0.84	n/a	2.69
	Customized	n/a	1.97	0.46	1.23	n/a	3.16
K7L	*Generic*	1.91	1.57	0.34	0.53	2.2	1.76
	Customized	2.11	1.91	0.19	0.39	2.14	2.08
K8L	*Generic*	1.51	1.63	0.21	0.87	1.96	2.50
	Customized	1.84	1.82	0.11	0.80	2.07	2.61
Mean ± std	*Generic*	1.43±0.3	1.59±0.19	0.35±0.21	0.73±0.16	2.06±0.12	2.1±0.50
	Customized	1.66±0.4	1.74±0.32	0.26±0.13	0.71±0.33	2.01±0.17	2.28±0.60
Gerus et al		2.09±0.44	1.78±0.35	1.3±0.82	0.64±0.29	n/a	n/a
Lerner et al		1.69±0.31	1.34±0.38	0.86±0.24	0.60±0.31	n/a	n/a
Nejad et al		n/a	n/a	n/a	n/a	2.64±0.58	
Dumas et al		1.73±0.24	1.39±0.37	0.54±0.18	0.51±0.11	1.96±0.36	1.88±0.37

Table S4:

		Medial	Lateral	Total
K1L	*Generic*	0.58	1.24	1.72
	Customized	0.75	1.50	2.21
K2L	*Generic*	0.63	1.98	2.6
	Customized	1.69	1.57	3.2
K3R	*Generic*	0.64	1.53	2.25
	Customized	0.98	1.27	2.25
K5R	*Generic*	1.12	1.86	2.9
	Customized	1.28	2.39	3.67
K7L	*Generic*	0.54	0.88	1.33
	Customized	0.54	0.87	1.33
K8L	*Generic*	0.84	1.50	2.14
	Customized	1.36	1.62	2.73
Mean ± std	*Generic*	0.73±0.22	1.50±0.40	2.16±0.57
	Customized	1.1±0.42	1.54±0.50	2.57±0.82
Schellenberg et al		n/a	n/a	3.70±0.64
Nejad et al		n/a	n/a	4.66±1.04
Nassab et al		n/a	n/a	3.86±0.86
Bedo et al		2.40	4.61	n/a
Dumas et al		1.26±0.47	0.82±0.42	1.94±0.33

Appendix A – Computational framework adapted from [14,40,51]

The musculoskeletal model of the lower limb used in the present study is identical to [51] except for the patella-femoral parameters and customization of knee muscle pathways. The model is parameterized with natural coordinates $\mathbf{Q}_i$, where each segment is defined by two unitary directional vectors and two position vectors [13]. It is composed of five segments: foot, shank, patella, thigh, and pelvis (i = 1, ..., 5). Muscle lever arms were computed using the muscle geometry of [10] adjusted so as to be subject-specific.

The kinematic constraints and the associated Jacobian matrix $\mathbf{K}^k$ are defined for each joint. As in [51], the tibiofemoral joint (T) is modeled with five kinematic constraints:

$$\boldsymbol{\phi}_T^k = \begin{pmatrix} \left(\mathbf{N}_4^{V_4^1}(\vartheta)\mathbf{Q}_4 - \mathbf{N}_2^{V_2^1}(\vartheta)\mathbf{Q}_2\right) \cdot \mathbf{N}_2^{\mathbf{X}_2}(\vartheta)\mathbf{Q}_2 \\ \left(\mathbf{N}_4^{V_4^1}(\vartheta)\mathbf{Q}_4 - \mathbf{N}_2^{V_2^1}(\vartheta)\mathbf{Q}_2\right) \cdot \mathbf{N}_2^{\mathbf{Y}_2}(\vartheta)\mathbf{Q}_2 \\ \left(\mathbf{N}_4^{V_4^1}(\vartheta)\mathbf{Q}_4 - \mathbf{N}_2^{V_2^1}(\vartheta)\mathbf{Q}_2\right) \cdot \mathbf{N}_2^{\mathbf{Z}_2}(\vartheta)\mathbf{Q}_2 \\ \left(\mathbf{N}_4^{V_4^2}(\vartheta)\mathbf{Q}_4 - \mathbf{N}_2^{V_2^2}(\vartheta)\mathbf{Q}_2\right) \cdot \mathbf{N}_2^{\mathbf{X}_2}(\vartheta)\mathbf{Q}_2 \\ \left(\mathbf{N}_4^{V_4^2}(\vartheta)\mathbf{Q}_4 - \mathbf{N}_2^{V_2^2}(\vartheta)\mathbf{Q}_2\right) \cdot \mathbf{N}_2^{\mathbf{Y}_2}(\vartheta)\mathbf{Q}_2 \end{pmatrix} \quad (1)$$

with $\mathbf{N}_i^{V_i^j}$ the interpolation matrix for the j^{th} virtual marker of the i^{th} segment depending on the tibiofemoral extension-flexion angle ϑ and with $\mathbf{N}_2^{\mathbf{X}_2}$; $\mathbf{N}_2^{\mathbf{Y}_2}$; $\mathbf{N}_2^{\mathbf{Z}_2}$ the interpolation matrices for the axes of the tibia segment coordinate system. The interpolation matrices, $\mathbf{N}$, allow the position of any point (or the orientation of any direction) embedded in the relevant segment to be determined from its natural coordinates $\mathbf{Q}_i$. Specifically, these virtual markers (i.e., V_2^1; V_2^2; V_4^1; and V_4^2) correspond to the medial and lateral contact points embedded in the shank and thigh segment, respectively. There are five kinematic constraints at each position in extension-flexion of the joint. The medial contact points of tibia and femur were superimposed in the three directions of space while the lateral contact points of tibia and

femur were superimposed only in the X (anterior-posterior) and Y (superior-inferior) directions of the shank.

Constrained multi-body kinematics optimization [17] is performed in order to obtain consistent segment positions $\mathbf{Q}$, velocities $\dot{\mathbf{Q}}$, and accelerations $\ddot{\mathbf{Q}}$. The optimization minimizes the sum of the squared differences between measured and model-derived skin marker trajectories:

$$\min_{\mathbf{Q}} f = \frac{1}{2}(\boldsymbol{\Phi}^m)^T \boldsymbol{\Phi}^m$$

$$\text{Subject to} \begin{pmatrix} \boldsymbol{\Phi}^k \\ \boldsymbol{\Phi}^r \end{pmatrix} = 0 \qquad (2)$$

$\boldsymbol{\Phi}^m$ represent the differences between measured and model-derived skin marker trajectories, $\boldsymbol{\Phi}^k$ are the kinematic constraints, and $\boldsymbol{\Phi}^r$ are the rigid body constraints detailed in [17].

Then, the inverse dynamics equation of the lower limb is written. In contrast with the classical approach, the dynamics equation of the whole kinematics chain is used here, introducing the musculo-tendon forces and the Lagrange multipliers.

$$[\mathbf{L} - \mathbf{K}^{\boldsymbol{T}}] \begin{pmatrix} \mathbf{f} \\ \boldsymbol{\lambda} \end{pmatrix} = \mathbf{G}\ddot{\mathbf{Q}} - \mathbf{R} - \mathbf{P} \qquad (3)$$

with **G** the generalized mass matrix, $\ddot{\mathbf{Q}}$ the consistent generalized accelerations, **P** the vector of generalised weights, **R** the vector of generalized ground reaction, **L** the vector of generalized muscular lever arms, $\mathbf{K} = [\mathbf{K}^k \ \mathbf{K}^r]$ the Jacobian matrix of both joint kinematics and rigid body constraints, **f** the vector of musculo-tendon forces, and $\boldsymbol{\lambda}$ the Lagrange multipliers.

Equation (3) gives direct access to the unknowns, consisting only of the musculo-tendon forces and the Lagrange multipliers corresponding straightforwardly to the joint contact, ligament, and bone forces.

Then, a partial reduction is introduced and one-step optimization is performed to solve the muscle redundancy problem:

$$\min_{\begin{pmatrix} f \\ \lambda_1 \end{pmatrix}} J = \frac{1}{2}\begin{pmatrix} \mathbf{f} \\ \boldsymbol{\lambda_1} \end{pmatrix}^T \mathbf{W} \begin{pmatrix} \mathbf{f} \\ \boldsymbol{\lambda_1} \end{pmatrix}$$

$$\text{Subject to } \begin{cases} \mathbf{Z}_{\mathbf{K}_2 T}[\mathbf{L} - \mathbf{K}_1^T]\begin{pmatrix} \mathbf{f} \\ \boldsymbol{\lambda_1} \end{pmatrix} = \mathbf{Z}_{\mathbf{K}_2 T}(\mathbf{G}\ddot{\mathbf{Q}} - \mathbf{R} - \mathbf{P}) \\ \begin{pmatrix} \mathbf{f} \\ \boldsymbol{\lambda_1} \end{pmatrix} \geq 0 \end{cases} \quad (4)$$

where $\boldsymbol{\lambda_1}$ are the Lagrange multipliers that we want to introduce into the objective function and $\mathbf{K}_1$ the associated Jacobian matrix, $\mathbf{Z}_{\mathbf{K}_2}$ is the projection matrix composed of the eigenvectors of the square matrix $\mathbf{K}_2^T\mathbf{K}_2$ that enables us to cancel other Lagrange multipliers $\boldsymbol{\lambda}_2$, and **W** is the optimization weights matrix.

When an optimization weight is not null, the associated force is minimized and constrained to be positive. Otherwise, for null optimization weight, the associated force is only constrained to be positive. The optimization weights used for this study are described below [40]:

	Selected Lagrange multipliers	Associated optimization weight
Musculo-tendon forces	All	1e0
Joint contact force	Hip X/Y/Z	1e0 / 1e0 / 1e0
	Medial tibiofemoral X/Y/Z	1e-6 / 2e0 / 1e-6
	Lateral tibiofemoral X/Y	1e-6 / 4e0
	Patellofemoral X /Y/Z	1e-6 / 0 / 0
	Ankle X/Y/Z	1e0 / 1e0 / 1e0
Ligament force	PT	1e-6
Bone forces	Femur	1e-6
	Tibia	1e-6

X: Anterior-Posterior, Y: Superior-Inferior, Z: Medio-Lateral